Progress In Electromagnetics Research, PIER 100, 37–54, 2010

HYBRID METHOD OF OBTAINING DEGREES OF FREEDOM FOR RADIAL AIRGAP LENGTH IN SRM UNDER NORMAL AND FAULTY CONDITIONS BASED ON MAGNETIOSTATIC MODEL

H. Torkaman and E. Afjei

Department of Electrical and Computer Engineering
Shahid Beheshti University, G.C.
Tehran, Iran

Abstract—In this paper, a new hybrid method of obtaining the degrees of freedom for redial airgap length in Switched Reluctance Motor operation under normal and faulty conditions based on magnetostatic analysis is presented. At the beginning, this method goes through the magnetic design of the motor utilizing three dimensional (3-D) Finite Element Method (FEM) in order to consider the end effects as well as axial fringing field effects. The motor parameters, such as torque, flux linkage, flux density versus rotor position are precisely obtained. Then, a Multi Layered Perception Neural Network is designed by considering the nonlinear behavior of the motor parameters obtained under different modes of operation. Using this network and the obtained parameters from FEM, an Objective Function (OF) for torque ripple with the aim of having a minimum mean square error is estimated. In addition, an improved Genetic Algorithm (GA) for the minimization the OF is also presented to determine the motor's operational regions. Finally, the legal intervals for different modes of motor operation are addressed.

1. INTRODUCTION

Switched Reluctance Motor (SRM) with its low-cost structure has only steel material for the rotor and stator, with concentrated windings on the stator, which makes an ideal choice for low-cost and high performance applications [1–4].

Corresponding author: H. Torkaman (H_Torkaman@sbu.ac.ir).

Recently optimized design technology focuses more on numerical methods, which has led to optimization of motor sizes as well as minimization of torque ripple [5, 6]. Electromagnetic motor design and optimization have been affected very much by utilizing computer-based methods that use evolutionary computational techniques [7], such as Genetic Algorithm (GA) [8–10], evolutionary programming and also numerical methods like Boundary Element Method (BEM) and Finite Element Method (FEM) implemented by authors in [11, 12].

GAs are stochastic search processes, based on fundamental principles of natural selection and genetic evolution. A method that GA uses for creating an individual vector, biologically called chromosome, which makes it different from the deterministic search processes [14–18].

The main performance of GA is based on composition, mutation, crossover and selection procedures [19–23, 38–43]. The use of this search algorithm was applied to optimizing torque ripple, which has led to finding the interval of airgap in faulty and healthy conditions. This algorithm is used in order to facilitate a parallel search in the parameters space using the genetic operands to obtain a group of coded chromosomes, which shows the system parameters in an optimized manner.

In the proposed hybrid method, for fitting the parameters by a non-linear function with suitable coefficients the Artificial Neural Network (ANN) is employed. ANN is one of the most popular and widely applied methods due to its superior ability of approximating unknown nonlinear function to any degree of desired accuracy. This method has been widely applied to many fields, such as image processing, pattern recognition, signal processing, and weather prediction, particularly in the area of the electromagnetics [24–26, 44–46].

Behavior analysis of any electrical system requires an accurate modeling of that system [27–31, 47–52]. In order to consider the real model of the motor and its operation in nonlinear states the exact parameters are required. Therefore, in this research, the three dimensional (3D) FEM is used to obtain the precise model of the SR motor.

The authors in the previous works modeled SRG [1, 11] and SRM [12, 13] in healthy and faulty [2, 3] modes utilizing three dimensional FEM. In this paper, the intervals for different modes of motor operation are calculated and presented by a different technique known as hybrid method.

2. PROBLEM STATEMENT

In high-power density motors the need for smaller air gap is one of the important requirements. Smaller airgap length will also force the motor into a highly saturated operation, accompanied by high radial forces causing mechanical vibration of stator core and housing in radial direction [32, 33]. Therefore, obtaining the optimum airgap length is essential for achievement of high performance motor.

One of the most common types of fault in electrical machine is the eccentricity fault. This type of fault is considered as abnormal condition and will be modeled in this paper. Occurrence of eccentricity fault leads to decreasing or increasing of the airgap length in different directions. These variations will change the motor parameters. Consequently, the boundary of radial airgap length variation must be calculated to attain smooth control on motor to achieve high performance expected from machine.

On the other side, the maximum and minimum variations of airgap must be obtained to determine the different modes of motor operation. Based on this matter the paper will introduce a new hybrid method in the next section. This method benefits from the advantages obtained by FEM, NN and GA techniques to develop the degrees of freedom for airgap length in SRM under normal and faulty conditions.

3. NEW METHOD OF IMPLEMENTATION AND RESULTS

At the beginning of this method, a three dimensional finite element analysis is being used to determine the magnetic field distribution in and around the motor. The MagNet package [34] has been used to analyze the magnetic field in order to determine the static torque at different rotor positions. This method considers the geometry of the motor to solve the magnetic field distribution in and around the motor. Other parameters of the motor such as flux density, flux linkage, coil inductance and static torque can be derived from resulted magnetic fields. The advantages of the 3-D FE method used in this algorithm over the 2-D FE method is the consideration of end effects and also axial fringing fields that lead to more accurate and real modeling of the motor. This has been explained comprehensively in the earlier study in [12].

There are two common methods for solving magnetic field problems. One utilizes magnetic vector potential A, and the other employs electric vector potential T. The partial differential equation for the magnetic vector potential is given by;

$$-\frac{\partial}{\partial x}\left(\gamma\frac{\partial A}{\partial x}\right)-\frac{\partial}{\partial y}\left(\gamma\frac{\partial A}{\partial y}\right)-\frac{\partial}{\partial z}\left(\gamma\frac{\partial A}{\partial z}\right)=J \qquad (1)$$

where, A is the magnetic vector potential.

In the variational method (Ritz) the solution to (1) obtained by minimizing the following function;

$$F(A)=\frac{1}{2}\iiint\limits_{\alpha}\left[\gamma\left(\frac{\partial A}{\partial x}\right)^2+\gamma\left(\frac{\partial A}{\partial y}\right)^2+\gamma\left(\frac{\partial A}{\partial z}\right)^2\right]d\alpha-\iiint\limits_{\alpha}JAd\alpha \qquad (2)$$

where α is the problem region of integration. The field analysis has been performed using a MagNet package which is based on the variational energy minimization technique to solve for the electric vector potential. In this method, electric vector potential known as $T-\Omega$ formulation in which T is defined by;

$$J=\nabla\times T \qquad (3)$$

From Maxwell's equation we have

$$\nabla\times H=J=\nabla\times T \qquad (4)$$

Then

$$\nabla\times(H-T)=0 \qquad (5)$$

Since the vector $(H-T)$ can be expressed as the gradient of a scalar, i.e.,

$$H=T-\nabla\Omega \qquad (6)$$

where Ω is a magnetic scalar potential.

And, since

$$\nabla\times E=-\frac{\partial B}{\partial t} \qquad (7)$$

Then,

$$\begin{aligned}\nabla\times E&=\nabla\times\left[\left(\frac{1}{\sigma}\right)\nabla\times T\right]=-\frac{\partial B}{\partial t}=-\mu_0\mu_r\left(\frac{\partial}{\partial t}\right)(T-\nabla\Omega)\\&=-\mu_0\mu_r\left(\frac{\partial T}{\partial t}\right)-\nabla\left(\frac{\partial\Omega}{\partial t}\right)\end{aligned} \qquad (8)$$

which finally reduces to the following two scalar equations

$$\nabla^2T-\mu\sigma\left(\frac{\partial T}{\partial t}\right)=-\mu\sigma\nabla\left(\frac{\partial\Omega}{\partial t}\right) \qquad (9)$$

And

$$\nabla^2\Omega=0 \qquad (10)$$

When a three dimensional magnetic field problem is solved by A and V, the need to solve for all the three components of A arises, whereas using the $T - \Omega$ method, T can be simplified to produce a solution with only two components of T.

For the present study, it has been assumed that each stator phase is excited with four-node tetrahedral blocks of current. Also, in this analysis, the usual assumptions such as the magnetic field outside an air box in which the motor is placed are considered to be zero.

The unaligned position is defined when the rotor pole is located across from the stator slot in such a way that the reluctance of the motor magnetic structure is at its maximum. This position is considered to be at zero degree in the motor performance plot. The aligned position is defined when the rotor pole is fully opposite to the stator pole, in which the reluctance of the motor magnetic structure is at its minimum supposed to happen at 44 degree. A 6/4 switched reluctance motor is depicted in Fig. 1 and will be analyzed using three dimensional finite element (Fig. 2).

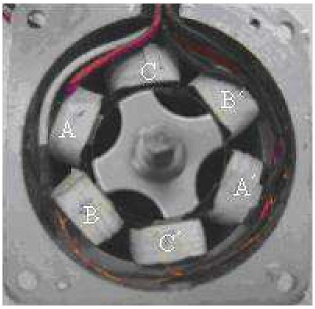

Figure 1. The front view of a three phase 6/4 SRM.

The SR motor dimensions used in this paper are: Stator core outer diameter: 72 mm, Rotor core outer diameter: 40.5 mm, Length of air gap: 0.25 mm, Shaft diameter: 10 mm, Number of turns: 120, Rotor pole arc: 32° and Stator pole arc: 28°. The motor model (stator and rotor cores) is made of M-27 non-oriented silicon steel laminations with static B-H curve as depicted in Fig. 3.

The rated motor phase current is at 2.5 Ampere and is used for simulation for the initial design parameters. This motor is considered running in counterclockwise direction. The 3D FE method results in magnetic flux density, torque and flux linkage for different rotor positions from unaligned to aligned positions. The next step considers a new condition which has been placed on the length of the airgap according to different rotor eccentricity levels shown in Fig. 4. Now

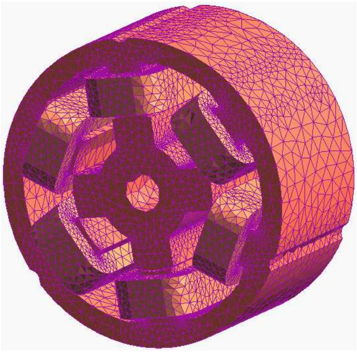

(a)

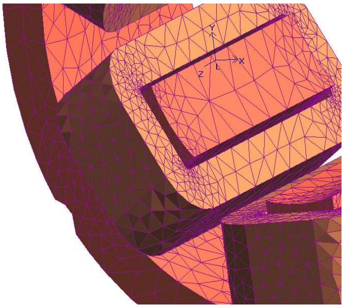

(b)

Figure 2. (a) Finite element mesh for the 6/4 SRM. (b) Zoomed mesh for one coil.

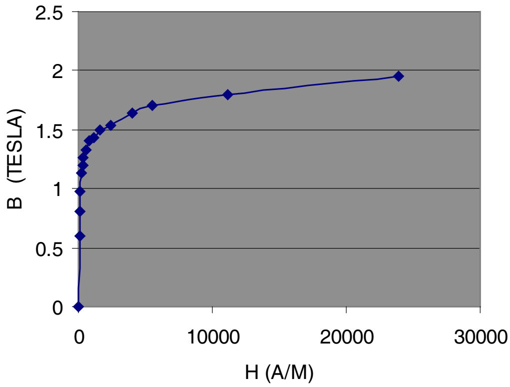

Figure 3. Magnetization curve for M-27 non-oriented silicon steel sheet.

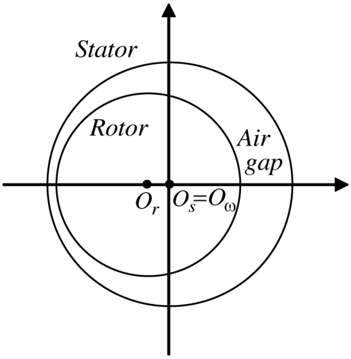

Figure 4. Schematic of motor with changes in air-gap length (Dynamic Eccentricity).

again, the different motor parameters for the new condition are obtained. Using these values, the OF will be developed. Using this OF, the region of the motor's operation in the healthy as well as eccentric modes (faulty mode) will be determined.

Dynamic eccentricity is a type of airgap non-uniformity in which airgap is time variant when dynamic eccentricity occurs. Therefore, the distribution of airgap changes when the rotor rotates. The degree of dynamic eccentricity fault is defined as follow:

$$\varepsilon_D = \left(\frac{O_\omega \times O_r}{g}\right) \times 100\,(\%) \tag{11}$$

where ε_D is the percentage of dynamic eccentricity between the stator and rotor axes; g is the radial airgap length in the case of uniform airgap in healthy motor or with no eccentricity. O_ω, O_r and O_s are the rotor rotation center, rotor symmetry center and stator symmetry center, respectively. Also, $(O_\omega \times O_r)$ is called the dynamic transfer vector.

The static torque developed by the motor is calculated from the ratio of change in the co-energy with respect to the rotor position. Regarding Eq. (5), the static torque versus rotor position for both healthy motor and the motor with various eccentricities utilizing 3-D FEM is obtained and shown in Fig. 5. This will be the first step of implementation of the hybrid method.

Due to higher flux linkages in a faulty motor, the static torque obtained is also higher than healthy motor. In addition, during the motoring operation the unbalanced magnetic pull tends to increase the dynamic eccentricity as well.

The percentage of variation of torque with occurrence of eccentricity is shown in Table 1. It can be observed that reducing the airgap length will increase the variations in torque profile in such way that when 10% eccentricity exists, the magnitude of the motor torque increases up to 4.3%.

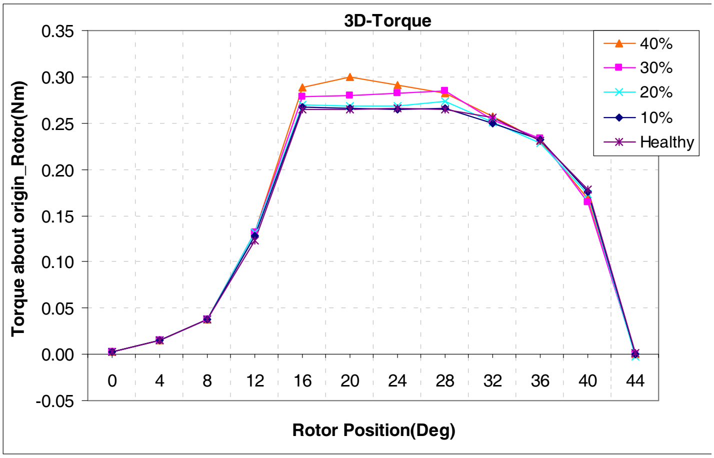

Figure 5. Static torque of the motor vs. rotor position for 3-D FEM: healthy motor and motor with various dynamic eccentricities.

Table 1. Percentage of variation of torque for healthy motor vs. motor with various eccentricities.

Degree	10% Eccentricity	20% Eccentricity	30% Eccentricity	40% Eccentricity
0	−0.64608	−1.04665	−0.60742	−0.65109
4	−0.13025	−0.18173	−1.34245	−0.56049
8	1.30615	1.40194	0.180424	0.032708
12	4.35884	7.0072	6.557116	6.978498
16	0.75793	1.93555	4.854805	8.779511
20	0.51967	1.35769	5.386814	13.28741
24	−0.51106	0.76182	5.820789	9.454833
28	0.71208	3.33119	7.427393	6.742136
32	−2.59001	−1.82419	−0.87997	0.419986
36	0.3212	−1.24276	0.870109	−0.48171
40	−1.43321	−2.87013	−8.18836	−5.0447
44	−1.82347	−2.41758	−3.96404	−3.42164

Table 2. Flux linkage in coil No. 1 in the first phase in motor and in healthy mode from unaligned to aligned positions.

Degree	Flux Linkage_Coil1 (mWb)
0	7.37073472
4	7.613212179
8	8.271031639
12	10.12098261
16	16.07182076
20	23.30779437
24	30.50245643
28	37.56267675
32	44.30275992
36	50.19602623
40	54.24661799
44	55.45333403

Table 3. Flux linkage in coil No. 1 in the first phase in motor and in healthy mode from aligned to unaligned positions.

Degree	Flux Linkage_Coil1 (mWb)
44	55.45333403
48	54.25251449
52	50.16700549
56	44.25771256
60	37.53474268
64	30.53563612
68	23.30838645
72	16.04502741
76	10.10249904
80	8.288291556
84	7.602377878

Also, in eccentric motor with 20%, 30% and 40% dynamic eccentricities, the torque profile produced 7%, 8.1% and 13.2% higher values, respectively.

Moreover, the uniformity of flux density distribution of the motor in healthy condition from front and lateral views is shown in Figs. 5(a) and (b), respectively. The values of flux linkage in coil No. 1 of the first phase are shown in Table 2 and Table 3 in healthy motor from unaligned position to aligned positions.

The next step in the hybrid method, obtained parameters from Finite Element Method, are imported to a MLP (Multi Layered Perceptron) Neural Network with one hidden layer of perceptron to compute a non-linear function (Eq. (6)) with suitable coefficients. This network consists of two layers as depicted in Fig. 7.

In this level of algorithm, the static torque is defined as a nonlinear function of rotor position, flux linkage and percentage of eccentricity (or the variations of airgap).

$$T = F\left(\theta, \varphi, \varepsilon_D\right) \tag{12}$$

Table 4. Values set and the mean square error average.

Result	Samples	MSE
Training	60%	2.6589e-4
Validating	20%	9.3837e-2
Testing	20%	5.5298e-2

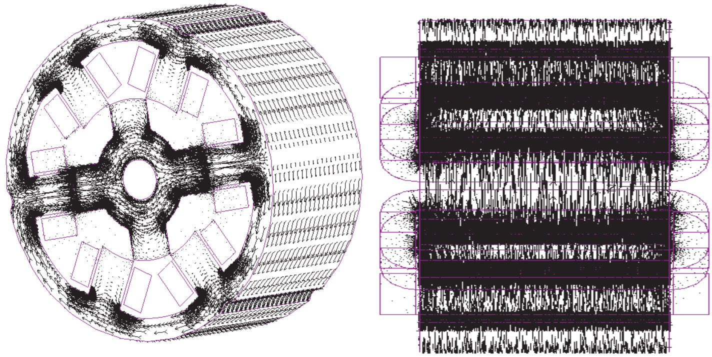

(a) (b)

Figure 6. Flux density distribution in SR motor in healthy condition. (a) Front view. (b) Lateral view.

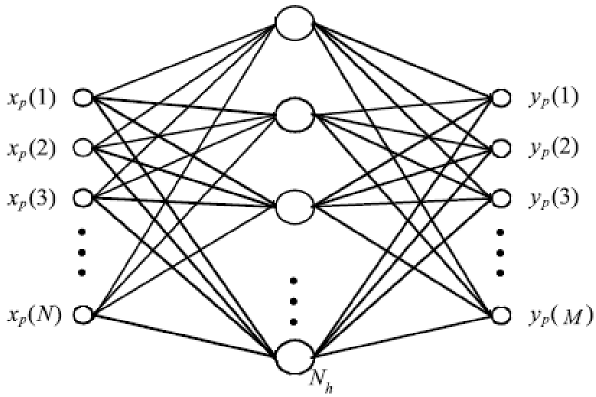

Figure 7. Network schematic to estimate the objective function.

where T is the static torque; θ is the rotor position; φ is the flux linkage; ε_D is the percentage of dynamic eccentricity.

The network is constructed according to some initial parameters as training pattern, with the weights assigned to each of them. The network is trained until a desirable mean square error (MSE) is obtained. For this network, 60% of the samples are employed for training; 20% are used for validation; 20% of the samples are spent for the test of the network. The number of neurons in the hidden layer is set to 20 using 4 input neurons for this network. The results are shown in Table 4.

In the next level of the new method, the neural network sends its function coefficients to Genetic Algorithm in which the objective function (OF) is defined as below:

$$OF = \text{Min}\,(\textit{Torque Ripple}\,\%) \tag{13}$$

Above equation represents the objective function by minimizing the amount of torque ripple based on the developed function from neural network. Also the torque ripple is defined as follow:

$$\textit{Torque Ripple}\,\% = \frac{T_{\max} - T_{\min}}{T_{\max}} \times 100\% \tag{14}$$

where $T_{\max}$ and $T_{\min}$ are the maximum and minimum static torque values, respectively. At the beginning of this step, the primary population consists of 100 chromosomes and is imported to objective function. Based on the torque ripple results as an optimized value, the superior points with more fitness are selected to continue the procedure of the algorithm. In the next step, mutation by Gaussian method is used to avoid trapping in a local minimum. In this method, a chromosome consists of two elements (x, σ), in which the x vector is defined as a point in search space, and the σ vector is the standard deviation. A new chromosome (x', σ') is produced as below:

$$\begin{cases} \sigma' = \sigma\, e^{N(0,\,\Delta\sigma)} \\ x' = x + N\,(0\,,\,\Delta\sigma') \end{cases} \tag{15}$$

where, $N(0, \Delta\sigma')$ is a vector for random Gaussian numbers with Mean value equals zero. The mutation operand changes the one gene from chromosome with 10% mutation rate.

Some chromosomes are selected for scattered type crossover to produce new generation of the chromosomes with new desirable features. The crossover rate is set to 60%. The new produced generation, which consists of flux linkage and airgap, will be sent to the beginning of the algorithm for the next level of the optimization.

Table 5. Range of torque values in different regions of motor operation.

Rotor Position (Degree)	Healthy Operation (0–9% eccentricity)		Faulty Operation (9–65% eccentricity)		Destructive Operation ($\varepsilon > 65\%$ eccentricity)	
	Min	Max	Min	Max	Min	Max
0	0.0026	0.0028	0.0028	0.0032	0.0032	> 0.0032
4	0.0151	0.0153	0.0153	0.0164	0.0164	> 0.0164
8	0.0372	0.0378	0.0378	0.0395	0.0395	> 0.0395
12	0.1228	0.1284	0.1284	0.1414	0.1414	> 0.1414
16	0.2648	0.2668	0.2668	0.2982	0.2982	> 0.2982
20	0.2646	0.2660	0.2660	0.3098	0.3098	> 0.3098
24	0.2650	0.2663	0.2663	0.3115	0.3115	> 0.3115
28	0.2641	0.2660	0.2660	0.2999	0.2999	> 0.2999
32	0.2557	0.2492	0.2492	0.2898	0.2898	> 0.2898
36	0.2303	0.2322	0.2322	0.2335	0.2335	> 0.2335
40	0.1688	0.1753	0.1753	0.1888	0.1888	> 0.1888
44	0.0000	0.0003	0.0003	0.0004	0.0004	> 0.0004

This procedure will continue until it reaches the maximum number of the produced generation, which is 2000 in this case.

The results concluded from the algorithm show the minimum and maximum airgap lengths for the motor operation. In other words, the legal intervals of motor operation in the occurrence of eccentricity fault

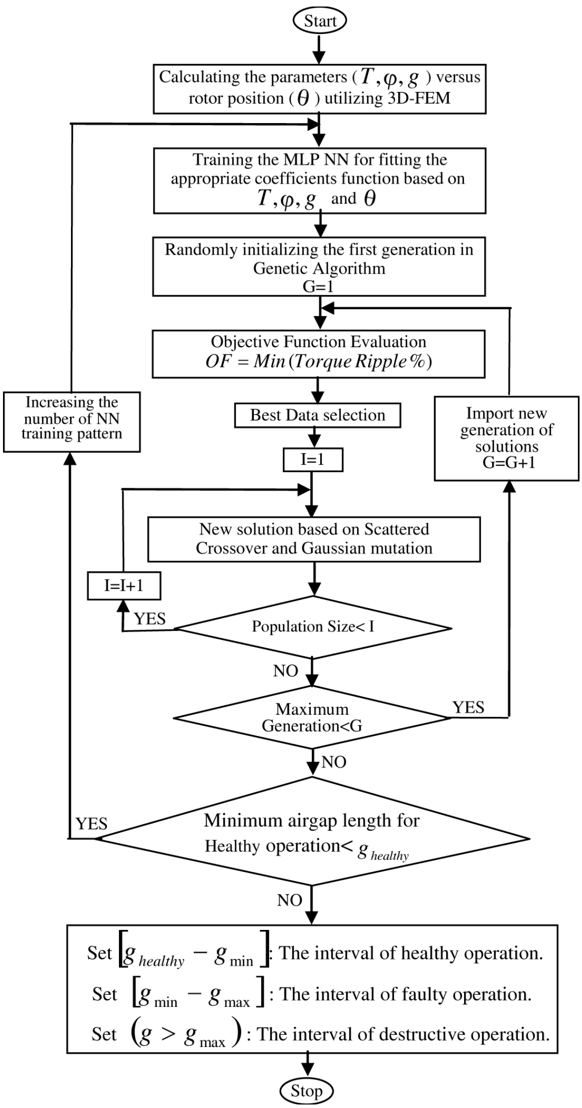

Figure 8. Hybrid method flowchart.

are calculated. In order to obtain the maximum legal intervals from eccentricity fault, the maximum value of objective function is used. The flowchart of this hybrid method is shown in Fig. 8.

According to the results obtained from the new method, it can be observed that the motor under 0% eccentricity to 9% eccentricity can be named as healthy motor, or [0%–9%] eccentricity interval is defined for healthy operation. The interval between 9% to 65% can be named as the interval of motor's operation in faulty condition. It is necessary to correct the motor's operation using electrical or mechanical controls under faulty condition. The interval higher than 65% can be named as motor's destructive interval in which the motor has no ability to continue to rotate under load and the crash of the rotor, and the stator is very probable. The motor should be repaired or serviced in this condition. The three intervals for motor operation under eccentricity fault from manufacturing companies indicate 0–10% for healthy motor, 10–50% for faulty motor, and more than 50% is considered as the destructive interval of motor operation [35–37].

Table 5 shows the range of operation obtained for healthy, faulty, and destructive intervals and their corresponding torque values for these three regions from unaligned to aligned positions.

4. CONCLUSION

A new procedure named hybrid method for computing the degrees of freedom of airgap in SRM under faulty and healthy conditions based on magnetostatic analysis has been proposed and analyzed. It computes the legal intervals for the radial airgap length as well as the regions of the motor's operation under different conditions. In the hybrid algorithm a 6/4 switched reluctance motor utilizing 3-D FEM has been designed and analyzed, then motor's parameters including torque with maximum of 0.28 N.m are achieved. The SR motor is then faced with eccentricity fault ranging from 0% to 70% in 5% steps. The resulted parameters are imported to a MLP neural network to produce the characteristic function as well as an objective function for torque ripple. In this study, 60% of the samples are used for training purposes, 20% for validating and the remaining 20% for testing the estimated function. The parameters of the non-linear equation for torque ripples are given to GA as an objective function, and then the algorithm computes the optimized parameters and also the optimized intervals based on minimization of torque ripple. Reducing the airgap length will result in an increase in torque variations in a way such that it will have an increase of 13.28% in maximum and 4.3% in minimum levels. 0% up to 9% eccentricity is named as the legal interval of the healthy motor operating condition. In other words, the variations of airgap length are acceptable in this range for normal operation of the motor. The region of the faulty motor is defined while motor operates with 9% up to 65% eccentricity. More than 65% eccentricity fault leads to motor entrance into the destructive operation interval in which the motor is not suitable for the operation anymore.

REFERENCES

1. Afjei, E. and H. Torkaman, "The novel two phase field-assisted hybrid SRG: Magnetio static field analysis, simulation, and experimental confirmation," *Progress In Electromagnetics Research B*, Vol. 18, 25–42, 2009.
2. Torkaman, H. and E. Afjei, "Magnetio static field analysis regarding the effects of dynamic eccentricity in switched reluctance motor," *Progress In Electromagnetics Research M*, Vol. 8, 163–180, 2009.
3. Torkaman, H. and E. Afjei, "Comprehensive magnetic field based study on effects of static rotor eccentricity in switched reluctance motor parameters utilizing three dimensional finite element," *Electromagnetics Journal*, Vol. 29, No. 5, 421–433, Taylor and Francis, 2009.
4. Hudson, C. A., N. S. Lobo, and R. Krishnan, "Sensorless control of single switch-based switched reluctance motor drive using neural network," *IEEE Transaction on Industrial Electronics*, Vol. 55, No. 1, 321–329, Jan. 2008.
5. Kano, Y., T. Kosaka, and N. Matsui, "Optimum design approach for two-phase switched reluctance compressor drive," *IEEE International Electric Machines* & *Drives Conference*, Vol. 1, 797–804, May 2007.
6. Morimoto, M., "Application specific permanent magnet motors and reluctance motors," *International Power Electronics Conference*, Vol. 1, 241–246, 2000.
7. Wieczorek, J., O. Gol, and Z. Michalewicz, "An evolutionary algorithm for the optimal design of induction motors," *IEEE Transaction on Magnetics*, Vol. 34, No. 6, 3882–3887, 1998.
8. Bianchi, N. and S. Bolognini, "Blushless DC motor design: An optimization procedure based on genetic algorithm," *Proc. of IEE EMD97*, No. 444, 16–20, 1997.
9. Chai, K. and C. Pollock, "Evolutionary computer controlled design of a reluctance motor drive system," *Proc. of IEEE/IAS Annual Meeting*, Vol. 3, 1480–1487, 2003.

10. Cho, D., H. Jung, and C. Lee, "Induction motor design for electric vehicle using a niching genetic algorithm," *IEEE Transaction on Industry Applications*, Vol. 37, No. 4, 994–999, 2001.
11. Afjei, E., A. Seydatan, and H. Torkaman, "A new two phase bidirectional hybrid switched reluctance motor/field-assisted generator," *Journal of Applied Science*, Vol. 9, No. 4, 765–770, 2009.
12. Torkaman, H. and E. Afjei, "Comprehensive study of 2-D and 3-D finite element analysis of a switched reluctance motor," *Journal of Applied Science*, Vol. 8, No. 15, 2758–2763, 2008.
13. Afjei, E. and H. A. Toliyat, "A novel multilayer switched reluctance motor," *IEEE Transaction on Energy Conversion*, Vol. 17, No. 2, 217–221, 2002.
14. Owatchaiphong, S., C. Carstensen, and R. De Doncker, "Optimization of predesign of switched reluctance machines cross section using genetic algorithms," *7th International Conference on Power Electronics and Drive Systems (PEDS'07)*, 707–711, Nov. 2007.
15. Agastra, E., G. Bellaveglia, L. Lucci, R. Nesti, G. Pelosi, G. Ruggerini, and S. Selleri, "Genetic algorithm optimization of high-efficiency wide-band multimodal square horns for discrete lenses," *Progress In Electromagnetics Research*, PIER 83, 335–352, 2008.
16. Meng, Z., "Autonomous genetic algorithm for functional optimization," *Progress In Electromagnetics Research*, PIER 72, 253–268, 2007.
17. Mahanti, G. K., N. Pathak, and P. Mahanti, "Synthesis of thinned linear antenna arrays with fixed sidelobe level using real-coded genetic algorithm," *Progress In Electromagnetics Research*, PIER 75, 319–328, 2007.
18. Rostami, A. and A. Yazdanpanah-Goharriz, "A new method for classification and identification of complex fiber bragg grating using the genetic algorithm," *Progress In Electromagnetics Research*, PIER 75, 329–356, 2007.
19. Elmas, C. and T. Yigit, "Genetic algorithm based on-line tuning of a PI controller for a switched reluctance motor drive," *Electric Power Components and Systems Journal*, Vol. 35, No. 6, 675–691, Taylor & Francis, Jun. 2007.
20. Riabi, M. L., R. Thabet, and M. Belmeguenai, "Rigorous design and efficient optimizattion of quarter-wave transformers in metallic circular waveguides using the mode-matching method and the genetic algorithm," *Progress In Electromagnetics Research*,

PIER 68, 15–33, 2007.

21. Xu, Z., H. Li, Q.-Z. Liu, and J.-Y. Li, "Pattern synthesis of conformal antenna array by the hybrid genetic algorithm," *Progress In Electromagnetics Research*, PIER 79, 75–90, 2008.
22. Mahanti, G. K., A. Chakraborty, and S. Das, "Phase-only and amplitude-phase only synthesis of dual-beam pattern linear antenna arrays using floating-point genetic algorithms," *Progress In Electromagnetics Research*, PIER 68, 247–259, 2007.
23. Chen, X., K. Huang, and X.-B. Xu, "Microwave imaging of buried inhomogeneous objects using parallel genetic algorithm combined with FDTD method," *Progress In Electromagnetics Research*, PIER 53, 283–298, 2005.
24. Zhang, Y.-D. and L. Wu, "Weights optimization of neural network via improved BCO approach," *Progress In Electromagnetics Research*, PIER 83, 185–198, 2008.
25. Li, X. and J. Gao, "Pad modeling by using artificial neural network," *Progress In Electromagnetics Research*, PIER 74, 167–180, 2007.
26. Bermani, E., S. Caorsi, and M. Raffetto, "An inverse scattering approach based on a neural network technique for the detection of dielectric cylinders buried in a lossy half-space," *Progress In Electromagnetics Research*, PIER 26, 67–87, 2000.
27. Vaseghi, B., N. Takorabet, and F. Meibody-Tabar, "Transient finite element analysis of induction machines with stator winding turn fault," *Progress In Electromagnetics Research*, PIER 95, 1–18, 2009.
28. Chari, M. V. K., G. Bedrosian, J. D'Angelo, A. konrad, G. M. Cotzas, and M. R. Shah, "Electromagnetic field analysis for electrical machine design," *Progress In Electromagnetics Research*, PIER 4, 159–211, 1991.
29. Shiri, A. and A. Shoulaie, "A new methodology for magnetic force calculations between planar spiral coils," *Progress In Electromagnetics Research*, PIER 95, 39–57, 2009.
30. Ravaud, R. and G. Lemarquand, "Comparison of the coulombian and amperian current models for calculating the magnetic field produced by radially magnetized arc-shaped permanent magnets," *Progress In Electromagnetics Research*, PIER 95, 309–327, 2009.
31. Ravaud, R., G. Lemarquand, V. Lemarquand, and C. Depollier, "The three exact components of the magnetic field created by a radially magnetized tile permanent magnet," *Progress In Electromagnetics Research*, PIER 88, 307–319, 2008.

32. Li, J., D. Choi, and Y. Cho, "Analysis of rotor eccentricity in switched reluctance motor with parallel winding using FEM," *IEEE Transactions on Magnetics*, Vol. 45, No. 6, 2851–2854, 2009.
33. Cameron, D. E., et al., "The origin and reduction of acoustic noise in doubly salient variable-reluctance motors," *IEEE Transaction on Industrial Application*, Vol. 28, No. 6, 1250–1255, Nov./Dec. 1992.
34. MagNet CAD package: User manual, Infolytica Corporation Ltd., Montreal, Canada, Jan. 2007.
35. Guldemir, H., "Detection of air-gap eccentricity using line current spectrum of induction motors," *Electric Power Systems Research Journal*, Vol. 64, 109–117, Elsevier, 2003.
36. Sheth, N. K. and K. R. Rajagopal, "Effects of nonuniform air-gap on the torque characteristics of a switched reluctance motor," *IEEE Transactions on Magnetics*, Vol. 40, No. 4, 2032–2034, Jul. 2004.
37. Nandi, S., H. A. Toliyat, and X. D. Li, "Condition monitoring and fault diagnosis of electrical motors — A review," *IEEE Transactions on Energy Conversion*, Vol. 20, No. 4, 719–729, Dec. 2005.
38. Liu, B., L. Beghou, L. Pichon, and F. Costa, "Adaptive genetic algorithm based source identification with near-field scanning method," *Progress In Electromagnetics Research B*, Vol. 9, 215–230, 2008.
39. Chen, H. T., G.-Q. Zhu, and S.-Y. He, "Using genetic algorithm to reduce the radar cross section of three-dimensional anisotropic impedance object," *Progress In Electromagnetics Research B*, Vol. 9, 231–248, 2008.
40. Ngo Nyobe, E. and E. Pemha, "Shape optimization using genetic algorithms and laser beam propagation for the determination of the diffusion coefficient in a hot turbulent jet of air," *Progress In Electromagnetics Research B*, Vol. 4, 211–221, 2008.
41. Tokan, F. and F. Gunes, "The multi-objective optimization of non- uniform linear phased arrays using the genetic algorithm," *Progress In Electromagnetics Research B*, Vol. 17, 135–151, 2009.
42. Panduro, M. A., C. A. Brizuela, L. I. Balderas, and D. A. Acosta, "A comparison of genetic algorithms, particle swarm optimization and the differential evolution method for the design of scannable circular antenna arrays," *Progress In Electromagnetics Research B*, Vol. 13, 171–186, 2009.
43. Su, D. Y., D.-M. Fu, and D. Yu, "Genetic algorithms and method

of moments for the design of pifas," *Progress In Electromagnetics Research Letters*, Vol. 1, 9–18, 2008.

44. Zainud-Deen, S. H., H. A. El-Azem Malhat, K. H. Awadalla, and E. S. El-Hadad, "Direction of arrival and state of polarization estimation using radial basis function neural network (Rbfnn)," *Progress In Electromagnetics Research B*, Vol. 2, 137–150, 2008.
45. Singh, D., V. Srivastava, B. Pandey, and D. Bhimsaria, "Application of neural network with error correlation and time evolution for retrieval of soil moisture and other vegetation variables," *Progress In Electromagnetics Research B*, Vol. 15, 245–465, 2009.
46. Castaldi, G., V. Galdi, and G. Gerini, "Evaluation of a neural-network-based adaptive beamforming scheme with magnitude-only constraints," *Progress In Electromagnetics Research B*, Vol. 11, 1–14, 2009.
47. Panda, D. K. K., A. Chakraborty, and S. R. Choudhury, "Analysis of co-channel interference at waveguide joints using multiple cavity modeling technique," *Progress In Electromagnetics Research Letters*, Vol. 4, 91–98, 2008.
48. Lu, H. H., C. H. Lee, P. W. Ko, C. H. Kuo, C. C. Liu, H. B. Wu, and J. S. Shin, "Direct-detection bidirectional radio-on-DWDM transport systems," *Journal of Electromagnetic Waves and Applications*, Vol. 23, No. 7, 875–884, 2009.
49. Zhang, Y.-J. and E.-P. Li, "Scattering of three-dimensional chiral objects above a perfect conducting plane by hybrid finite element method," *Journal of Electromagnetic Waves and Applications*, Vol. 19, No. 11, 1535–1546, 2005.
50. Pingenot, J., R. N. Rieben, D. A. White, and D. G. Dudley, "Full wave analysis of RF signal attenuation in a lossy rough surface cave using a high order time domain vector finite element method," *Journal of Electromagnetic Waves and Applications*, Vol. 20, No. 12, 1695–1705, 2006.
51. Ozgun, O. and M. Kuzuoglu, "Finite element analysis of electromagnetic scattering problems via iterative leap-field domain decomposition method," *Journal of Electromagnetic Waves and Applications*, Vol. 22, No. 2–3, 251–266, 2008.
52. Zhang, Y., X. Wei, and E. Li, "Electromagnetic scattering from threedimensional bianisotropic objects using hybrid finite element-boundary integral method," *Journal of Electromagnetic Waves and Applications*, Vol. 18, No. 11, 1549–1563, 2004.